energies

MDPI

Article

Multi-Objective Optimization of a Hybrid Nanogrid/Microgrid: Application to Desert Camps in Hafr Al-Batin

Houssem Rafik Al-Hana Bouchekara [1,*], Mohammad Shoaib Shahriar [1], Muhammad Sharjeel Javaid [1], Yusuf Abubakar Sha'aban [1] and Makbul Anwari Muhammad Ramli [2]

[1] Department of Electrical Engineering, University of Hafr Al-Batin, Hafr Al-Batin 31991, Saudi Arabia; mshoaib@uhb.edu.sa (M.S.S.); javaid@uhb.edu.sa (M.S.J.); shaaban@uhb.edu.sa (Y.A.S.)

[2] Department of Electrical and Computer Engineering, King Abdulaziz University, Jeddah 21589, Saudi Arabia; mramli@kau.edu.sa

* Correspondence: bouchekara.houssem@gmail.com

Abstract: This paper presents an optimal design for a nanogrid/microgrid for desert camps in the city of Hafr Al-Batin in Saudi Arabia. The camps were designed to operate as separate nanogrids or to operate as an interconnected microgrid. The hybrid nanogrid/microgrid considered in this paper consists of a solar system, storage batteries, diesel generators, inverter, and load components. To offer the designer/operator various choices, the problem was formulated as a multi-objective optimization problem considering two objective functions, namely: the cost of electricity (COE) and the loss of power supply probability (LPSP). Furthermore, various component models were implemented, which offer a variety of equipment compilation possibilities. The formulated problem was then solved using the multi-objective evolutionary algorithm, based on both dominance and decomposition (MOEA/DD). Two cases were investigated corresponding to the two proposed modes of operation, i.e., nanogrid operation mode and microgrid operation mode. The microgrid was designed considering the interconnection of four nanogrids. The obtained Pareto front (PF) was reported for each case and the solutions forming this front were discussed. Based on this investigation, the designer/operator can select the most appropriate solution from the available set of solutions using his experience and other factors, e.g., budget, availability of equipment and customer-specific requirements. Furthermore, to assess the quality of the solutions found using the MOEA/DD, three different methods were used, and their results compared with the MOEA/DD. It was found that the MOEA/DD obtained better results (nondominated solutions), especially for the microgrid operation mode.

Keywords: desert camps; diesel generator; nanogrid; microgrid; multi-objective evolutionary algorithm; multi-objective optimization; solar energy

check for updates

Citation: Bouchekara, H.R.A.-H.; Shahriar, M.S.; Javaid, M.S.; Sha'aban, Y.A.; Ramli, M.A.M. Multi-Objective Optimization of a Hybrid Nanogrid/Microgrid: Application to Desert Camps in Hafr Al-Batin. *Energies* **2021**, *14*, 1245. https://doi.org/10.3390/en14051245

Academic Editor: Azeddine Houari

Received: 3 February 2021
Accepted: 16 February 2021
Published: 24 February 2021

Publisher's Note: MDPI stays neutral with regard to jurisdictional claims in published maps and institutional affiliations.

Copyright: © 2021 by the authors. Licensee MDPI, Basel, Switzerland. This article is an open access article distributed under the terms and conditions of the Creative Commons Attribution (CC BY) license (https://creativecommons.org/licenses/by/4.0/).

1. Introduction

A robust power grid is a vital element that ensures the sustained supply of electrical power to all customers connected to the grid, with low cost, better quality, and minimal environmental harm [1]. Establishing such a grid is very challenging in a centralized system because of long-distance transmission lines, which increase the outage threat. Moreover, factors like high carbon emission levels, high transmission losses, and the challenge of entertaining remote consumers have called reliance on an extensive grid system into question. The distributed generation (DG) concept has provided an alternative to such a situation; it deregulates highly interconnected power systems and takes care of the issues described above. This approach could significantly reduce transmission loss and increase system efficiency [2,3]. The microgrid concept is one of the DG implementation outcomes, which aims to ensure the optimal power supply to connected loads [4]. Integration of renewable energy sources like solar and wind in microgrids ensures the mitigation of environmental effects. It also helps control the power flow and eases connection with

the main grid [5]. A nanogrid is essentially a scaled-down version of a microgrid, and has received significant attention from researchers for its promising prospects in power system engineering.

The nanogrid is a single electrical power distribution domain in terms of capacity, voltage profile, expense, control strategy, and overall administration. This distribution system is usually used for one consumer: a single-unit house, a small-scale load or a small building [6]. The factors which make a nanogrid divergent from other minigrids are: consumer size, power rating, load size, complexity, hardware configuration, and control strategy. The margin of these factors between a nanogrid and other grids is still debated and nicely presented by Burmester et al. [6]. In a nanogrid system, there must be a local unit of power production. It can be a renewable source or a fossil fuel-dependent one. A hybrid nanogrid (HN) is a single unit of nanogrid in which different power production sources are present simultaneously. Such a unit is often connected to other neighboring grids by a gateway channel. Any sort of storage device is used in the nanogrid to ensure the stability of the system. Important technoeconomical parameters—cost of energy, storage cost, annual life cycle cost etc.—directly influence the storage devices chosen [7]. A controller, also known as the brain of a nanogrid, must be present, in order to coordinate the necessary operational strategies [8].

The classification of a nanogrid can be made via several factors. One of them is the type of transferred energy in the network—DC or AC. DC distribution offers better efficiency than AC despite some limitations [9]. Among the sources of energy, both renewable (solar, wind, biogas) and traditional (diesel, fuel cell) forms can be used [10]. However, to ensure the desired energy flow, suitable converters are widely used in both AC and DC grid systems.

Several methods are presented and discussed in the literature to optimize the size and operation of the nanogrid. A mixed-integer linear programming (MILP)-based algorithm was proposed by Atia et al. [11], which successfully optimized a residential load-connected hybrid nanogrid. This approach has a significant advantage: easy calculation. A hybrid grid system was optimized with a MILP-based multi-objective optimization problem [12]. Both the renewable and traditional sources were presented, and the fuzzy model searched for the optimal solution. Moreover, this paper's problem formulation included the cost-emission factor to reduce energy cost and CO_2 emission. For a small power system to support a ship, a similar approach was addressed by Lan et al. [13], including the optimal navigation of route tracking. Lokeshgupta et al. [14] offered an optimal energy management system, where a multi-objective optimization strategy simultaneously reduced the energy bill and the peak load. A decision support mechanism was proposed by Li et al. [15] to optimize the nanogrid, where the problem formulation was made by an augmented–constrained method. The characteristics and behavior of every unit of a hybrid network were well discussed by Hosseinalizadeh et al. [16]. The formulation complexity and optimization time were significantly reduced by linear programming formulation [17] while dealing with many variables. In a recent article [18], the branch-and-cut approach was proposed to search the Pareto front (PF) solution of the multi-objective problem. The paper addressed the issue of real-time variation of energy demand in a nanogrid.

A multi-objective approach was proposed by Brandoni et al. [18], where different load demand scenarios are considered in the load demand. The matter of climate classification was used to optimize a grid-connected system by Shivam et al. [19], and the authors investigated the issue in four different Taiwanese regions. A study was carried out in Savannah, Georgia, USA in which the impact of grid-connected nanogrids in tropical climates was discussed [20]. The article [21] presented a geographical map for optimally installing the standalone and grid-connected systems. It summarized that Cambridge Bay's location (in Canada) was the most suitable place from an economic point of view, whereas Toamasina was the optimal location in terms of energy efficiency. Voltage quality improvements [22] in a nanogrid system and cybersecurity insurance [23] were also addressed in some recent

articles. The review article [24] gathered all the relevant works on nanogrid optimization and demonstrated a critical comparison among the attempted approaches.

Camping is a part of tradition and culture in all the gulf countries; the Kingdom of Saudi Arabia (KSA) is not an exception. Camps are established in the desert, as a large portion of the countryside is covered by bare desert land. Al-Falahi et al. and Hilden et al. [24,25] demonstrated life in a desert tent, along with the life of tribal citizens of KSA. Some tents are built for a limited period, mostly during the winter season. In contrast, some are built for an extended period, mainly to graze domestic livestock. The temporary tents are primarily established for recreation, where local people spend time with their family and friends in cold weather. This paper used Hafr Al-Batin city, located in the Eastern Province of Saudi Arabia, to study the effect of nanogrids in a desert camp. Many tent-establishing shops in the city enjoy patronage in winter, selling and setting up hundreds of tents in the desert. However, current practices utilize diesel generators in these tents, which has evident shortcomings, e.g., high cost and negative environmental impact. These tents can be considered nanogrids. Upgrading such energy-consuming units by integrating a renewable energy source has vast potential. This upgrade is what we propose in this paper. This approach is suitable for any city or country, where desert camps are present. This paper presents an optimization strategy for a single nanogrid and proposes combining multiple nanogrids to form a microgrid—and operate them optimally. Even though much research has already been conducted on grid optimization, this paper will fill the gap by addressing the practical application in desert camps, where both the concepts of nanogrids and microgrids are concurrently implemented.

A multi-objective evolutionary algorithm is used in this paper to solve the complex multi-objective optimization of the nanogrid model. This algorithm offers an acceptable balance between diversity and convergence [26]. Several optimization techniques are noted in the literature, with a shortcoming: successfully dealing with multi-objective problems is more difficult than accounting for only two or three objectives. However, this paper's adopted technique is free from such drawbacks and effectively combines the properties of dominance and decomposition. Separately, dominance [27] and decomposition-based [28,29] evolutionary techniques have been used in the literature to deal with similar problems of microgrid characteristic optimization.

The main contribution of this paper is the optimal design of a smart grid, which can be modeled as a nanogrid or microgrid, depending upon the size of the desert camp load. This was achieved as follows: first, we formulated the nanogrid/microgrid design as a multi-objective problem. Second, we solved this problem using a performant multi-objective evolutionary algorithm based on dominance and decomposition—which has not been used before to solve a similar problem. Another contribution of this paper is the adoption of a variety of models for each equipment. The combination of these equipment models will lead to better results than the traditional use of a single model for each equipment.

The remaining paper is organized as follows: the subsequent section presents the fundamentals of the problem formulation. The description of the case study is discussed in Section 4. The detailed solution strategy of the addressed problem is explained in Section 5. Section 6 discusses the attained results with the necessary explanation. Finally, Section 7 concludes the paper.

2. System Description

In this section, the components of a typical nanogrid system and their respective models are discussed. A discussion on battery management strategy follows. The nanogrid formed by the primary constituents (Figure 1) was then extended to create a microgrid, as shown in Figure 2. An algorithm encompassing all possible conditions that a nanogrid (with available constituents) might encounter during daily operation is presented. The optimization problem is formulated in the subsequent section. The formulation developed in this work independently found the optimal design and size for standalone nanogrids, as well as microgrids formed by the interconnection of several nanogrids. Below, the

fundamental constituents of the system under study are explained and modeled. All these underlying components integrate to create a basic nanogrid. These multiple nanogrids are then connected to form an isolated nanogrid that shares their resources to ensure collective benefit within the newly formed microgrid. The term "hybrid" indicates that all discussed systems are composed of renewable and nonrenewable energy resources.

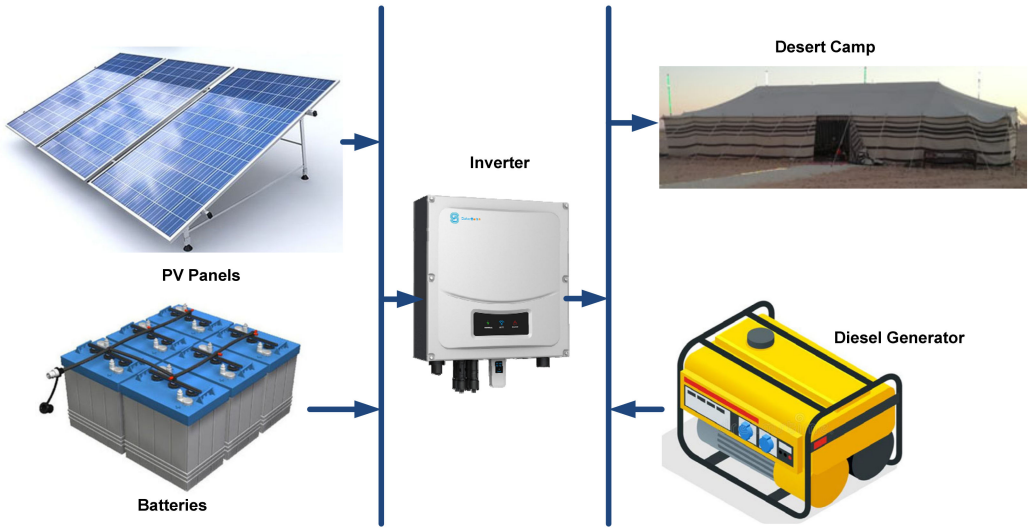

Figure 1. Standalone hybrid nanogrid for a desert camp.

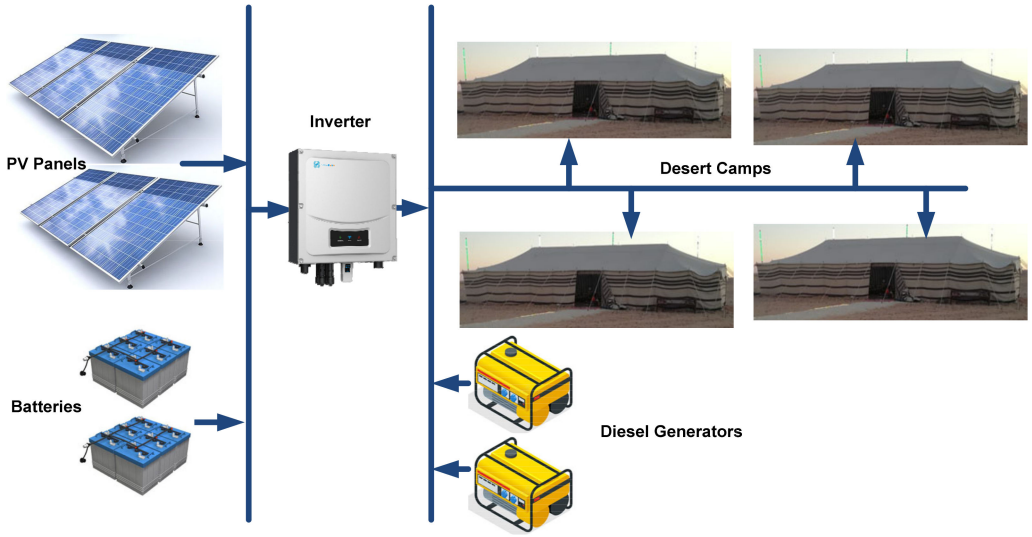

Figure 2. Standalone hybrid microgrid made up of multiple nanogrid for a desert camp.

2.1. Fundamental Constituents

The nanogrid under consideration was categorized as a standalone hybrid nanogrid composed of Photovoltaic (PV) panels, battery bank, DC/AC inverter, diesel generator, and a load representing the needs of a remote but fully equipped desert camp or tent [30]. Figure 1 illustrates the schematic of the nanogrid under consideration, while Figure 2 represents a microgrid's schematic formed by the interconnection of nanogrids. The details of each component are discussed.

PV systems have always been considered a noiseless, readily available and environmentally friendly energy resource [31]. In recent years, there has been a notable rise

in worldwide deployment. Conforming to global trends, KSA has envisioned a solar contribution amounting to 40 GW by 2030 to reduce fossil fuel dependency under the government's Vision 2030 [32]. Moreover, the country enjoys year-round solar availability and an extended summer season.

Daud et al. [33] and Razmjoo et al. [34] presented a way to compute a PV panel's output power, P_{PV-out}, given the instantaneous solar radiation, G (W/m^2), and ambient temperature, T_{amb} (°C), as shown below:

$$P_{PV-out} = P_{Rated} \times \frac{G}{G_r}\left[1 + K_t\Big((T_{amb} + (0.0256 \times G)) - T_{ref}\Big)\right] \quad (1)$$

where: K_t is a constant equal to -3.7×10^{-3} (1/°C), G_r is the reference value G taken to be of 1 kW/m^2 and P_{Rated} is the rated photovoltaic power at standard test conditions (STC). The temperature of the PV cell at STC, denoted by T_{ref}, is 25 °C.

In a hybrid nanogrid system, the diesel generator acts as the secondary source, conducive to reducing energy storage requirements, and plays a pivotal role in nanogrid economics, stability, and reliability. Due to its dependency on fossil fuel and low energy conversion efficiency, a diesel generator works at a low loading rate. Consequently, it is operated at peak load demand when the battery is depleted, making it an unlikely option under light loading conditions [35].

The diesel generator output is modelled by Ashari et al. in [36] where the fuel consumption of a diesel generator *s(t)* can be defined as a function of generated power, *P(t)*, and rated power, P_{rated}, as given below:

$$s(t) = x\ P(t) + y\ P_{rated} \quad (2)$$

where x and y with values of 0.246 and 0.08415, respectively, represent consumption coefficients [37].

The efficiency of the diesel generator, η_d, plays a crucial role in the model accuracy and is the function of thermal break efficiency, η_{bt}, and generator efficiency, η_g, as defined below:

$$\eta_d = \eta_{bt} \times \eta_g \quad (3)$$

In designing a hybrid nanogrid, the size of the battery plays a crucial role. Souraki et al. [38] and Parida et al. [39] highlighted three factors in determining suitable battery size. The first one was autonomy days (*AD*), defined as the number of consecutive days the desired load can be driven solely by the battery bank, without any external support. The second factor, the depth of discharge, M_{DD} (battery's maximum usable capacity), directly influences battery life. As a common practice, the battery of the system was designed with 40–80% of its regular discharge. The third factor, atmospheric temperature, displays a direct relationship with M_{DD}, i.e., the higher the temperature, the greater the battery's capacity, decreasing the battery's life and vice versa. To keep derate-factor, K_D, equal to one, the batteries are recommended to be kept at 25 °C.

The equation that relates all these factors in order to give battery bank capacity in Ah is given below:

$$B_C = \frac{L_{Ah}.\ AD}{M_{DD}.\ K_D} \quad (4)$$

where L_{Ah} is the Ah accumulated over a single day, having a unit of Ah/day.

The number of parallel battery banks, N_{BP}, is calculated by dividing targeted capacity, B_R with selected capacity, B_S as given below:

$$N_{BP} = \frac{B_R}{B_S} \quad (5)$$

In contrast, the number of series-connected batteries, N_{BS}, utilizes V_S and V_B, the DC voltage levels of system and battery, respectively:

$$N_{BS} = \frac{V_S}{V_B} \tag{6}$$

Finally, the total number of required batteries, N_B, is the product of N_{BP} and N_{BS}, as given below:

$$N_B = N_{BP} \,.\, N_{BS} \tag{7}$$

Consequently, if C_B denotes the cost of one battery, the cumulative battery bank cost, C_{Bank}, will become:

$$C_{Bank} = N_B \,.\, C_B \tag{8}$$

The last component enabling the conversion and power transfer between the AC and DC components of a hybrid nanogrid is the DC to AC inverter. A standalone hybrid system often requires a single inverter; however, mathematically, the precise number of inverters servicing a nanogrid, N_{inv_alone}, can be computed by a simple equation given below:

$$N_{inv\_alone} = \frac{P_{load}}{P_{inv}} \tag{9}$$

where P_{load} and P_{inv} represent the maximum load power and maximum inverter power capability, respectively. Discussion of the number of required inverters becomes vital when smaller networks are connected to form a more extensive network [40]. Consequently, if P_{Hyb} denotes the maximum power exchanged by a hybrid system, its ration with P_{inv} gives the number of required inverters in a grid connected system, N_{inv_grid}:

$$N_{inv\_grid} = \frac{P_{Hyb}}{P_{inv}} \tag{10}$$

2.2. Energy Management Strategy

The intrinsic intermittency and uncertainty in both solar and load profiles requires the development of an energy management strategy for a hybrid nanogrid. In this work, condition-based energy management is proposed. These conditions act as a precursor in the optimization framework and are listed below:

Condition 1: PV panels are the primary source of energy that is utilized with top priority.

Condition 2: If PV power is greater than the load, batteries are charged with the surplus power.

Condition 3: If PV and batteries combined are unable to supply the load, the diesel generator will compensate for deficit power.

Condition 4: If batteries are full, and PV has more power than required by the load, a dump load will be used to deal with the surplus power.

It is pertinent to represent these conditions in the form of a working algorithm. A framework comprising of nested if-else statements provide the workflow for the optimization formulation solved in the subsequent section. Algorithm 1 describes this framework with due linguistic convenience.

Algorithm 1: Conditions-based priority workflow to manage energy in a nanogrid/microgrid.

IF *PV panels instantaneous output is more than the instantaneous load,* **THEN**
energize all loads with PV output
IF *battery is not full,* ***THEN***
charge the batteries with surplus power
EISE *(battery is full)*
redirect the surplus power to the dumping load
END IF
ELSE *(Insufficient power at PV panels' output)*
IF *battery is full,* ***THEN***
use battery to share the load with the PV panels
IF *battery alone is insufficient,* ***THEN***
utilize the diesel generator along with the battery's available output
END IF
ELSE *(If the battery is depleted)*
rely entirely on the diesel generator to run all loads
END IF
END IF

3. Problem Formulation

The optimal sizing problem of nanogrid/microgrid constituents is formulated under the multi-objective framework [29] as follows:

$$\text{Minimize } \mathbf{F}(\mathbf{x}) = [f_1(\mathbf{x}),\ f_2(\mathbf{x})] \tag{11}$$

$$\text{Subject to } \mathrm{g}(\mathbf{x}) = 0 \tag{12}$$

$$\text{and } \mathrm{h}(\mathbf{x}) \leq 0 \tag{13}$$

where $f_1(\mathbf{x})$ and $f_2(\mathbf{x})$ are the cost of electricity (COE) and the loss of power supply probability ($LPSP$), respectively, while $\mathbf{x}$ represents the set of design variables. The variable $\mathrm{g}(\mathbf{x})$ denotes the set of equality constraints, whereas $\mathrm{h}(\mathbf{x})$ comprises all inequality constraints. The objective function aims to obtain a diverse set of nondominated solutions in vector **x,** known as the PF, simultaneously satisfying both equality and inequality constraints while looking for the best possible combination of solutions.

3.1. Objective Functions

COE and $LPSP$ are the two contrasting objectives of this problem. Various performance indicators assess the cost-effectiveness of a hybrid nanogrid/microgrid system. COE is one of the most common indices representing the per unit energy cost. It is evaluated using the following equation [41]:

$$COE = \frac{Total\_Cost}{\sum_{h=1}^{h=8760} P_{load}} \times CRF \tag{14}$$

$Total\_Cost$ in the numerator consists of all significant operational costs incurred by a system, including replacement cost, and maintenance cost. P_{load} in the denominator represents power consumption per hour and is accumulated over one year (8760 h) to give the cost per unit. Lastly, to incorporate the cost deterioration caused by the system's usage, the expression is multiplied by the capacity recovery factor (CRF). If n denotes

the life period of the PV panel—considered equal to the entire system's lifetime—and i incorporates the effect of interest rate, CRF would be:

$$CRF = \frac{i(i+1)^n}{(i+1)^n - 1} \tag{15}$$

Next, the intrinsic uncertainty of a PV panel is handled as the second objective function. Due to unanticipated interruptions in the solar availability and errors in the forecast, the system might fail to supply the required instantaneous demand. Therefore, such power supply failure becomes a probabilistic event measured through $LPSP$. $LPSP$ can be determined by running chronological simulations. Another approach to determine $LPSP$, used by Yang et al. [42] and Wang et al. [43], requires calculating the combined effect of all constituents of a nanogrid/microgrid. The chronological approach is used in this research, and the $LPSP$ is defined as follows [43]:

$$LPSP = \frac{\sum_{t=0}^{T} \text{Power.Failure.Time}}{\text{T}} \tag{16}$$

where T is the number of hours in this research. The power failure time is defined as the time that the load is not satisfied—when the power generated by the PV array is insufficient and the storage is depleted in [42].

It is worth mentioning that, although two objective functions have been considered for this study, many other objectives can be considered for future studies, including: minimization of emissions and pollutants, minimization of net present cost, and minimization of life cycle cost.

3.2. Design Variables

To enhance the optimization search space, manufacturing models of inverters, batteries, and PV panels are included as adjunct design variables. This feature enables the designer/operator of the hybrid system to select the most suitable manufacturer from each item's available list. Fundamentally, it provides the opportunity to choose the best combination of inverters, batteries and PV panels to work together to optimize COE and $LPSP$ of Equation (11). These adjunct design variables, representing various manufacturing models of PV panels, batteries, and inverters, are denoted by PV_{Model}, $\text{Battery}_{\text{Model}}$, and $\text{Inverter}_{\text{Model}}$, respectively, and are annexed to the existing list of design variables, $\mathbf{x}$, as shown below:

$$\mathbf{x} = \left[\text{NDG, NPV, AD, } \text{PV}_{\text{Model}}, \text{Battery}_{\text{Model}}, \text{Inverter}_{\text{Model}}\right] \tag{17}$$

NDG is the number of diesel generators, NPV is the number of PV panels, and AD is the number of autonomy days.

3.3. Constraints

The problem is constrained due to battery storage dynamics, as under:

$$\text{E}_{\text{Battery}}^{\text{min}} \leq \text{E}_{\text{Battery}}^{\text{i}} \leq \text{E}_{\text{Battery}}^{\text{max}} \tag{18}$$

$$\text{E}_{\text{Battery}}^{\text{min}} = (1 - \text{DOD})\text{C}_{\text{Battery}} \tag{19}$$

where $\text{E}_{\text{Battery}}^{i}$ represents the energy stored in the battery at the i^{th} hour, DOD represents the depth of discharge for the battery to protect the battery from over-discharge (set at 80% for this study), $\text{E}_{\text{Battery}}^{\text{min}}$ and $\text{E}_{\text{Battery}}^{\text{max}}$ are the minimum and maximum battery energy storage capacity, respectively.

4. Description of the Case Study

The countries of the Arabian Peninsula are naturally blessed with considerable solar resources. These countries have made significant efforts to utilize solar energy's copious resources [44]. Despite ample solar energy potential, KSA is still harnessing fossil fuel resources to meet energy demand. However, policymakers have noted the issue with care and are targeting the maximum use of renewable resources in the near future [45]. Figure 3 presents the horizontal solar irradiation data for the country of Saudi Arabia.

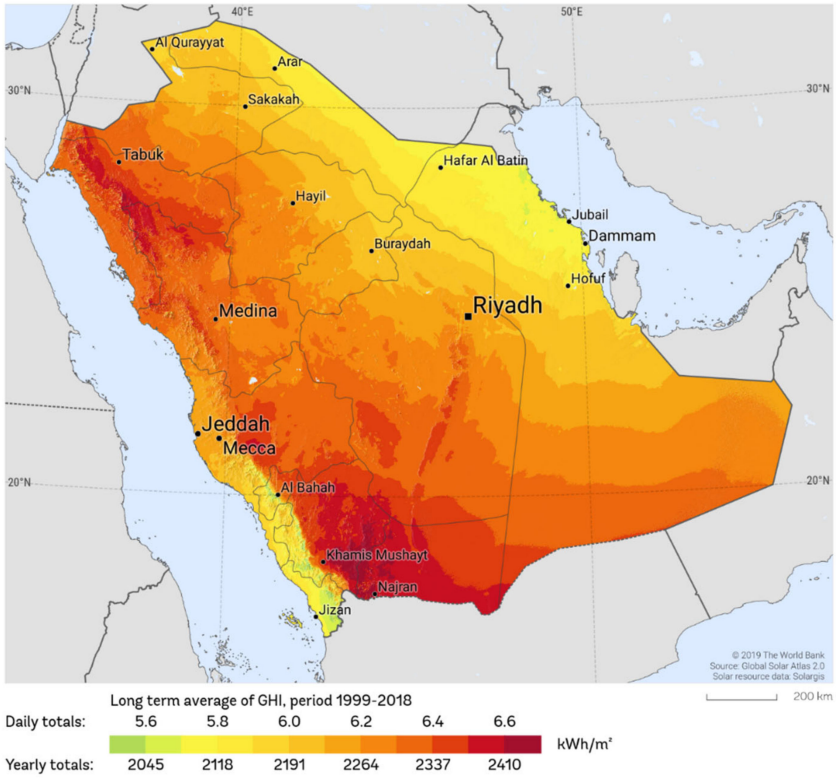

Figure 3. Global horizontal irradiation in Saudi Arabia [46].

Hafr Al-Batin is an important city in the Eastern Province of Saudi Arabia that shares a border with the neighboring country of Kuwait. This city has an extended winter season and is famous for desert camping activities. Most tents for these activities are supported by diesel generators and pollute the environment by burning fossil fuel. The average horizontal irradiation per day for this city is about 5.8 kWh/m^2, as shown in Figure 3 [46]. The hourly solar irradiation data is presented in Figure 4 [47].

Load Estimation for a Desert Camp

A desert camp may include several tents. As informed by an experienced local person, a typical camp may have up to 2 or 3 tents as living rooms, two washrooms, and one tent for the watchman. It may include surrounding fences. Table 1 summarizes the detail of all the electric loads usually present in a desert camp. In this table, the load was estimated by investigating a similar tent in the mentioned city. The average energy demands in a day were 30.93 kWh and 72.46 kWh for weekdays and weekends, respectively, as shown in the table. The total load of the camp was around 6.46 kW. The peak demand in the weekdays was 2.6 kW whereas it was 4.5 kW during the weekend. On weekdays, people may leave the tent in the morning, go to work, and return at dusk. Therefore, the demand for a typical weekday differs from a weekend day, when people often remain in the camp throughout the day. Figure 5 shows such a desert camp, whereas Figure 6 presents the estimated load variation per day for weekdays and weekends.

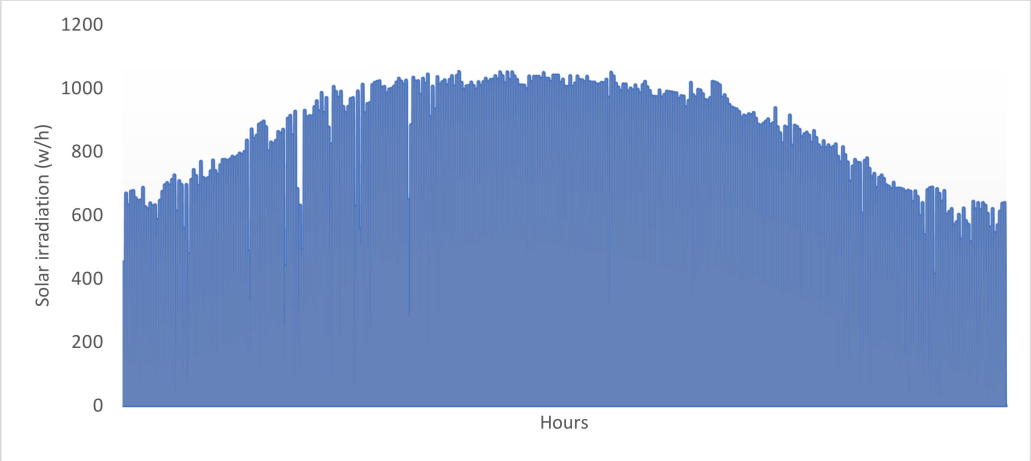

Figure 4. Solar irradiation per hour for Hafr Al-Batin city [48].

Table 1. Daily load demand details for a remote desert camp in Hafr al-Batin.

Appliance	Load (KW)	Quantity	Hours/Weekday	Hours/Weekend
Toaster	0.16	1	0	1
Ceiling fans	0.45	3	2	13
Cellular Charger	0.026	3	3	4
Laptop computer	0.101	2	2	10
TV Flat screen LCD 46	0.045	2	7	9
Tent light	0.04	12	13	13
Fence lights Type 1	0.04	10	11	11
Fence lights Type 2	0.01	20	10	10
Fence lights Type 2	0.025	10	10	10
Air conditioner	1.129	1	7	10
Air conditioner	1.129	1	0	19
Refrigerator	0.065	3	16	15
Vacuum Cleaner	0.8	1	1	1

Figure 5. A typical desert camp in Hafr Al-Batin.

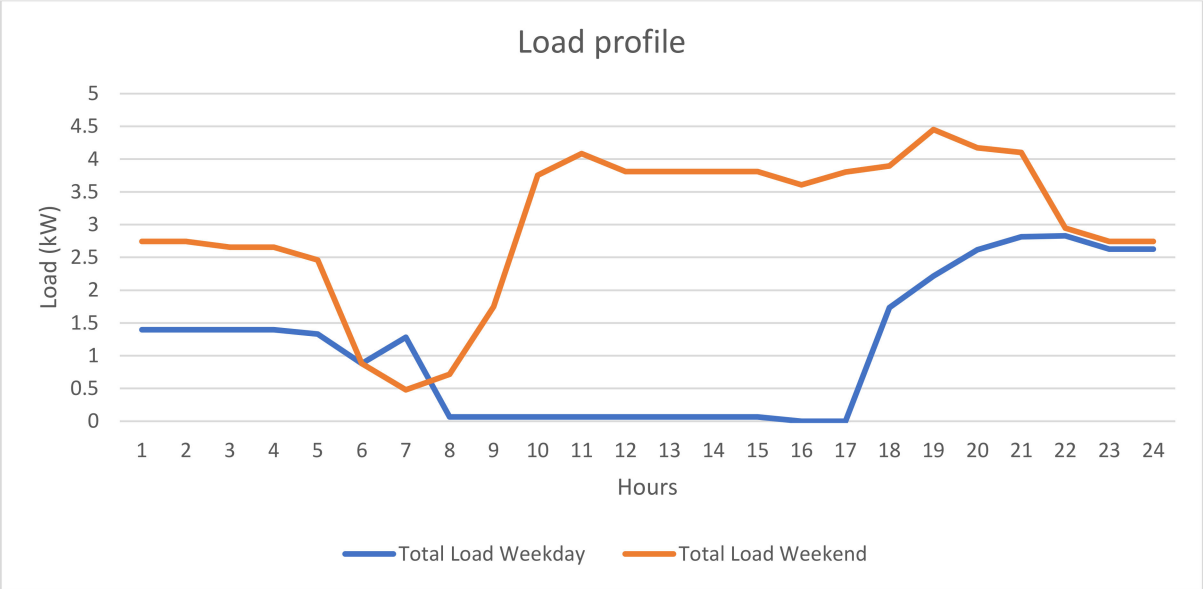

Figure 6. Load profile for a weekday and weekend day of a typical desert camp.

5. Problem Solution Approach

The approach proposed in this paper optimized the sizing of hybrid photovoltaic /diesel/battery nanogrids using a multi-objective evolutionary algorithm based on both dominance and decomposition (MOEA/DD) [26]. To solve the multi-objective problem presented in (11), MOEA/DD decomposed the problem into several scalar subproblems using classic multi-objective optimization approaches, e.g., the weighted sum, weighted Tchebycheff, and boundary intersection methods [29]. The penalty-based boundary intersection (PBI) approach, known for good performance on a large class of optimization problems, was adopted in this work [48,49].

The algorithm for MOEA/DD is presented in Algorithm 2 [26]. The MOEA/DD algorithm was initialized by generating N initial solutions and their corresponding weights. The parent population was then updated using elite-preserving mechanisms—offspring generated from parents through a mating procedure. In general, MOEA/DD is made up of the initialization, reproduction, and update procedures.

The initialization procedure (Algorithm 3) began with randomly sampling for the initial parent population P from Ω $(= \mathrm{g}(\mathbf{x})\mathrm{U}f(\boldsymbol{x}))$, uniformly distributed. This step was followed by the identification of the nondomination level structure of P, after which a set of weight vectors was generated before the assignment of the neighborhood. Weight generation methods discussed in [46,47] were associated with the explosion of computational complexity and diversity reduction, respectively. As such, the two-layer weight vector generation, proposed by Li et al. [26] was adopted. First, the sets of weight vectors in the boundary ($B = \left\{\boldsymbol{b}^1, \ldots, \boldsymbol{b}^{N_1}\right\}$ and inside ($I = \left\{\boldsymbol{i}^1, \ldots, \boldsymbol{i}^{N_2}\right\}$ layers of a simplex were generated such that $N = N_1 + N_2$. A coordinate transformation was then adopted to reduce the coordinates of weight vectors in the inside layer. This allowed for the evaluation of the jth component of $i^k = \left(i_1^k, \ldots i_m^k\right)^T$, $k \in \{1, \ldots N_2\}$ according to:

$$i_j^k = \frac{1-\tau}{m} + \tau \times i_j^k \tag{20}$$

where $\tau \in \{0, 1\}$ represents the shrinkage factor and $j \in \{1, \ldots, m\}$. The set $(= \{w^1, w^2, \ldots, w^N\})$ was formed by combining B and I. The weight vectors,

$w^i = \left(w_1^i, \ldots, w_m^i\right)$ respectively defined unique subregions in the objective space, Φ^i:

$$\Phi^i = \left\{ \boldsymbol{F}(\boldsymbol{x}) \in \Re^m \middle| \boldsymbol{F}(\boldsymbol{x}),\ \boldsymbol{w}^j \right\} \tag{21}$$

where $\langle \boldsymbol{F}(\boldsymbol{x}),\ \boldsymbol{w}^j \rangle$. is the acute angle between $\boldsymbol{F}(\boldsymbol{x})$ and $\boldsymbol{w}^j$, $j = \{1, \ldots, N\}$, $x \in \Phi$. The neighborhood of each of the weight vectors $\boldsymbol{w}^i$, $i \in \{1, \ldots, N\}$ was made up of the T closest weight vectors in a Euclidean sense. The fast nondominated sorting method [50] was used to divide the solutions in P into nondomination levels $(\boldsymbol{F}_1, \ldots, \boldsymbol{F}_l,\ l \leq N)$. Finally, each solution in P was initially randomly associated with a unique subregion.

The primary role of the reproduction procedure, presented in Algorithm 3 [26], was to update the parent population after generat1ing offspring solutions. This update was achieved using two main steps: mating selection and variation operation. In the mating selection, some parents are selected for offspring generation from a neighborhood. Each solution is associated with a uniquely weight-specified subregion based on Euclidean distance in the method used. This association allowed for consideration of neighboring solutions from neighboring subregions before randomly selecting mating parents from the whole population when there were no associated solutions. As proposed by Li et al. in [26], this work adopted the binary crossover (SBX) [51] and polynomial mutation [52] for the variation operation. Any other genetic operator could also be used.

The generated offspring was used to update the parent population according to Algorithm 4 [26]. The algorithm involved identifying the subregion of the offspring solution x^C and combing with the parent population P to generate a hybrid population P'. The nondominated level structure of $P\prime$ was then determined using the method presented by Li et al. [53]. Other considerations for updating were adopted from [26]. The optimal values of hypermeters were determined by trial and error aided by experience working with evolutionary algorithms.

Algorithm 2: General Framework of multi-objective evolutionary algorithm based on both dominance and decomposition (MOEA/DD)

Output: P

1 $[P,\ W,\ E] \leftarrow$ INITIALIZATION();→ // P—Parent population, W—weight vector set, E—neighborhood index set.
2 **while** stopping criterion not fulfilled **do**
3 **for** $i \leftarrow 1$ **to** N **do**
4 $\overline{P} \leftarrow$ MATING_SELECTION $(E(i),\ P)$;
5 $S \leftarrow$ VARIATION $(\overline{P})$;
6 **foreach** $X^c \in S$ *do* // X^c is an offspring
7 $P \leftarrow$ UPDATE_POPULATION$(P,\ X^c)$
8 **end**
end
end
return P.

Algorithm 3: Mating Selection.

Input: $E(i)$, P
Output: $\overline{P}$
if rnd $> \delta$ **then**
Randomly choose k indices from $E(i)$
If no solution in the selected subregion **then**
Randomly choose k solutions from P to form $\overline{P}$;
else
Randomly choose k solutions from the selected subregions to form $\overline{P}$;
end
else
Randomly choose k solutions from P to form $\overline{P}$;
end
return $\overline{P}$

Algorithm 4. Update Procedure.

Input: P, X^C
Output: P
Find the subregion associated with X^c according to (6)
$P' \leftarrow PU\{X^c\}$
Update the nondomination level structure of $P\prime$
If $l = 1$ **then**
$x' \leftarrow$ LOCATE_WORST(P')
$P \leftarrow P'\backslash\{\boldsymbol{X\prime}\}$;
else
If $|\boldsymbol{F}_l| = 1$ then
Solution $\boldsymbol{X}^l$
If $\left|\Phi^l\right| > 1$ // Φ^l is the associated subregion of X^l
$P \leftarrow P\backslash\left\{X^l\right\}$;
else // $\left|\Phi^l\right| = 1$
$X' \leftarrow LOCATE\_WORST(P\prime) \rightarrow$
$P \leftarrow P' \setminus \{X'\}$
end
else
Identify the most crowded subregion Φ^h associated with those solutions in F_l
if $\left|\Phi^h\right| > 1$ **then**
Find the worst solution
$X' = argmax_{X\in\Phi^h} g^{pbi}\left(X\middle|W^h, z^*\right)$;
$P \leftarrow P' \setminus \{X'\}$;
else // $\left|\boldsymbol{\Phi}^h\right| = 1$
$X' \leftarrow$ LOCATE_WORST (P');
$P \leftarrow P' \setminus \{X'\}$
end
end
end
Update the nondominated level structure of P;
return P

6. Application, Results and Discussion

The details of the models used for PV panels, batteries and inverters are tabulated in Tables A1–A3 of the Appendix A, respectively. The design variables were constrained as follows: NPV $\in [2, 100]$, NDG $\in [1, 10]$, AD $\in [1, 3]$, PV.$_{\text{Model}} \in [1, 13]$, Battery$_{\text{Model}} \in [1, 27]$ and Inverter$_{\text{Model}} \in [1, 8]$.

The proposed approach was applied to the following two case studies using a population size of 100 for 200 iterations:

CASE 1: Nanogrid operation mode
CASE 2: Microgrid operation mode

The following subsections describe the investigated cases and discuss the obtained results with some analysis and recommendations.

6.1. CASE 1: Nanogrid Operation Mode

This case investigated the operation of each tent separately (i.e., as a nanogrid). The MOEA/DD was run to solve the formulated problem for this case, and the obtained Pareto front was plotted in Figure 7. In this figure, the MOEA/DD generated 23 solutions; all of which occured between (COE = 0.3396 $/kWh, LPSP = 0.3015%) and (COE = 0.5544 $/kWh, LPSP = 0.1946%). It can be seen that the designer/operator can use a variety of solutions for this case.

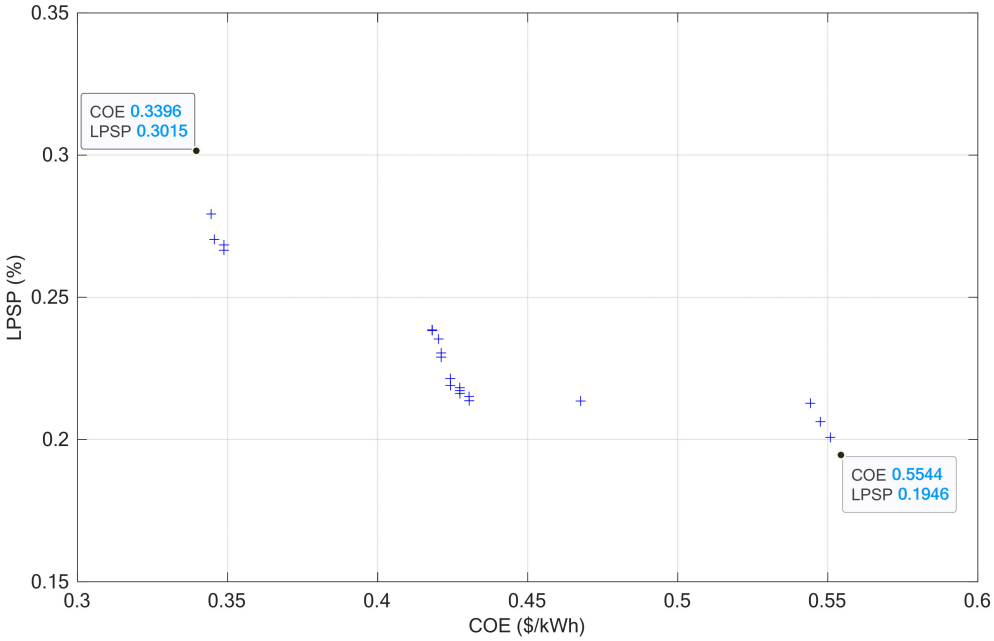

Figure 7. Pareto front (PF) obtained for CASE 1 using MOEA/DD.

In addition to that, the obtained PF solutions are given in Table 2. For convenience, these solutions are sorted in ascending order based on their COEs. If the designer/operator selects solution # 1, the nanogrid will be made of 2 PV panels and two diesel generators and will have an autonomy of 24 hours. The models for PV panel, battery and inverter are model # 7, model # 1 and model # 3, respectively, for this case. Finally, the objective functions obtained for this solution are COE = 0.3396 $/kWh and LPSP = 0.3015%.

A second example can be the selection of solution # 8. The designed nanogrid has an autonomy of more than 26 h. It comprises 13 PV panels (Model #1), two diesel generators, the PV panel, battery, and inverter model are model # 1, mode #5 and model # 3, respectively. This solution yields a COE of 0.4182 $/kWh and an LPSP of 0.2383%.

A third example can be illustrated by solution #23. The sized nanogrid, composed of 30 PV panels and two diesel generators, has more than 25 h of autonomy for this solution. The optimized component models are model #1, model #3 and model #3 for the PV panel, battery, and inverter, respectively. The solution has a COE of 0.5544 $/kWh and an LPSP of 0.1946%. The COE obtained for this solution is the most expensive due to the high number of PV panels used. Furthermore, Figure 8 exposes each component's contribution (i.e., PV panels, diesel generator, and battery) to the nanogrid over 50 h for solution #23.

Table 2. Solutions from PF for CASE 1.

Solution #	NPV	NDG	AD	PV_{Model}	$Battery_{Model}$	$Inverter_{Model}$	COE ($/kWh)	LPSP (%)
Solution 1	2	2	1.003	7	1	3	0.3396	0.3015
Solution 2	10	2	1.000	1	1	3	0.3445	0.2793
Solution 3	11	2	1.000	1	1	3	0.3456	0.2704
Solution 4	14	2	1.000	7	1	3	0.3488	0.2684
Solution 5	13	2	1.002	2	1	3	0.3488	0.2666
Solution 6	13	2	1.124	1	5	3	0.4182	0.2386
Solution 7	13	2	1.115	1	5	3	0.4182	0.2385
Solution 8	13	2	1.093	1	5	3	0.4182	0.2383
Solution 9	15	2	1.022	6	5	3	0.4203	0.2354
Solution 10	14	2	1.078	1	5	3	0.4212	0.2305
Solution 11	14	2	1.047	1	5	3	0.4212	0.2290
Solution 12	15	2	1.085	1	5	3	0.4242	0.2214
Solution 13	15	2	1.054	1	5	3	0.4243	0.2190
Solution 14	16	2	1.124	1	5	3	0.4274	0.2182
Solution 15	16	2	1.115	1	5	3	0.4274	0.2172
Solution 16	16	2	1.084	1	5	3	0.4274	0.2162
Solution 17	17	2	1.085	1	5	3	0.4305	0.2151
Solution 18	17	2	1.047	1	5	3	0.4305	0.2137
Solution 19	19	2	1.082	4	6	3	0.4677	0.2135
Solution 20	27	2	1.046	1	3	3	0.5442	0.2128
Solution 21	28	2	1.050	1	3	3	0.5475	0.2062
Solution 22	29	2	1.050	1	3	3	0.5509	0.2008
Solution 23	30	2	1.050	1	3	3	0.5544	0.1946

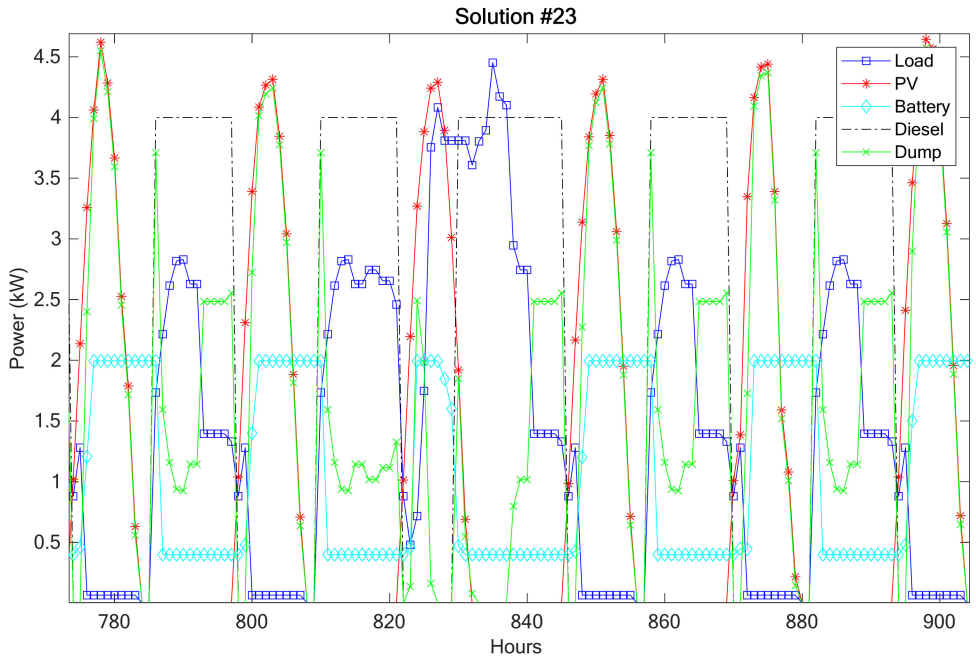

Figure 8. Zoom on the energy contribution of each component for solution #23.

6.2. CASE 2: Microgrid Operation Mode

In this second case study, four tents were connected to form one microgrid. The proposed approach based on MOEA/DD was applied to this case, and the obtained PF is plotted in Figure 9. The number of obtained solutions was 37, and they are well spread between the extreme points with the following objectives (COE = 0.1933 $/kWh, LPSP = 0.4541%) and (COE = 0.278 $/kWh, LPSP = 0.3028%). This solution offers the designer/operator many options to operate the tents together as a microgrid, instead of 4 separate nanogrids.

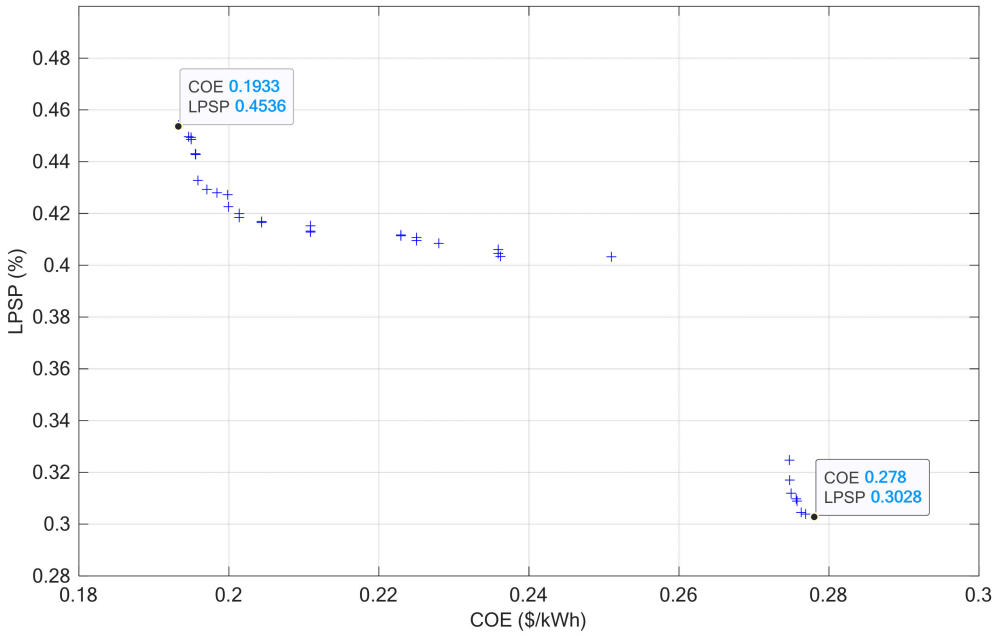

Figure 9. PF obtained for CASE 2 using MOEA/DD.

Furthermore, Table 3 tabulates the final set of PF solutions sorted in ascending COE-based order. Many options can be selected for this case. One option could be solution #1, where the resulting microgrid will be composed of 60 PV panels based on model # 1, and 5 diesel generators. The batteries have autonomy for almost one and a half days. The battery model #16 and inverter model #1 are the best options for this solution. The objective functions for this solution are COE = 0.1933 $/kWh and LPSP = 0.4541%.

Similarly, if solution #12 is selected, the microgrid will be composed of 77 PV panels, five diesel generators and the system will have an autonomy of fewer than 30 hours. For this solution scheme, the PV panel, battery, and inverter models are model #1, model #16, and model #1, respectively. The objective functions for this solution are COE = 0.1998 $/kWh and LPSP = 0.4272%.

Another solution could be solution #29. This solution is composed of 98 PV panels of model 1 and 5 diesel generators. The models for battery and inverter are model #16 and model #1, respectively.

It can also be seen from Table 3 that for almost all the cases the best models for PV panels are model #1, the best model among batteries is model #16, and the best model for the inverter is model #1.

Furthermore, solutions from 30 to 37 are not very acceptable. Although they are part of the PF numerically, they represent nonfeasible solutions.

Table 3. Solutions from PF for CASE 2.

Solution #	NPV	NDG	AD	PV_{Model}	$Battery_{Model}$	$Inverter_{Model}$	COE ($/kWh)	LPSP (%)
Solution 1	60	5	1.484	1	16	1	0.1933	0.4541
Solution 2	60	5	1.484	1	16	1	0.1933	0.4536
Solution 3	62	5	1.478	1	16	1	0.1946	0.4496
Solution 4	62	5	1.469	1	16	1	0.1949	0.4494
Solution 5	62	5	1.469	1	16	1	0.1950	0.4486
Solution 6	63	5	1.476	1	16	1	0.1955	0.4430
Solution 7	63	5	1.477	1	16	1	0.1956	0.4430
Solution 8	63	5	1.469	1	16	1	0.1956	0.4428
Solution 9	60	5	1.497	1	16	1	0.1959	0.4328
Solution 10	61	5	1.497	1	16	1	0.1971	0.4293
Solution 11	62	5	1.497	1	16	1	0.1984	0.4280
Solution 12	77	5	1.216	1	16	1	0.1998	0.4272
Solution 13	63	5	1.497	1	16	1	0.1999	0.4226
Solution 14	64	5	1.498	1	16	1	0.2014	0.4200
Solution 15	64	5	1.499	1	16	1	0.2014	0.4185
Solution 16	66	5	1.497	1	16	1	0.2044	0.4169
Solution 17	66	5	1.519	1	16	1	0.2044	0.4165
Solution 18	79	5	1.494	2	16	1	0.2109	0.4152
Solution 19	79	5	1.503	2	16	1	0.2109	0.4132
Solution 20	79	5	1.504	2	16	1	0.2109	0.4128
Solution 21	94	5	1.373	4	16	1	0.2229	0.4117
Solution 22	94	5	1.363	4	16	1	0.2229	0.4114
Solution 23	94	5	1.398	4	16	1	0.2250	0.4107
Solution 24	94	5	1.398	4	16	1	0.2250	0.4095
Solution 25	90	5	1.338	1	16	1	0.2280	0.4085
Solution 26	93	5	1.391	1	16	1	0.2359	0.4061
Solution 27	93	5	1.391	1	16	1	0.2359	0.4046
Solution 28	94	5	1.338	1	16	1	0.2362	0.4034
Solution 29	98	5	1.423	1	16	1	0.2510	0.4033
Solution 30	3	6	1.013	4	18	1	0.2747	0.3247
Solution 31	3	6	1.013	5	18	1	0.2748	0.3170
Solution 32	3	6	1.048	1	18	1	0.2750	0.3119
Solution 33	4	6	1.048	7	18	1	0.2756	0.3098
Solution 34	3	6	1.012	8	18	1	0.2757	0.3089
Solution 35	4	6	1.045	6	18	1	0.2763	0.3045
Solution 36	4	6	1.018	2	18	1	0.2769	0.3039
Solution 37	4	6	1.017	4	18	1	0.2780	0.3028

6.3. Comparative Study

A comparative study with other multi-objective optimization algorithms was conducted to assess the quality of the obtained results. Three well-known algorithms were selected for this study: (1) multi-objective evolutionary algorithm based on decomposition (MOEA/D), (2) novel multi-objective particle swarm optimization (NMPSO) and (3) speed-constrained multi-objective particle swarm optimization (SMPSO).

Figures 10 and 11 show the comparison of the PFs obtained using the four algorithms for CASE 1 and CASE 2, respectively.

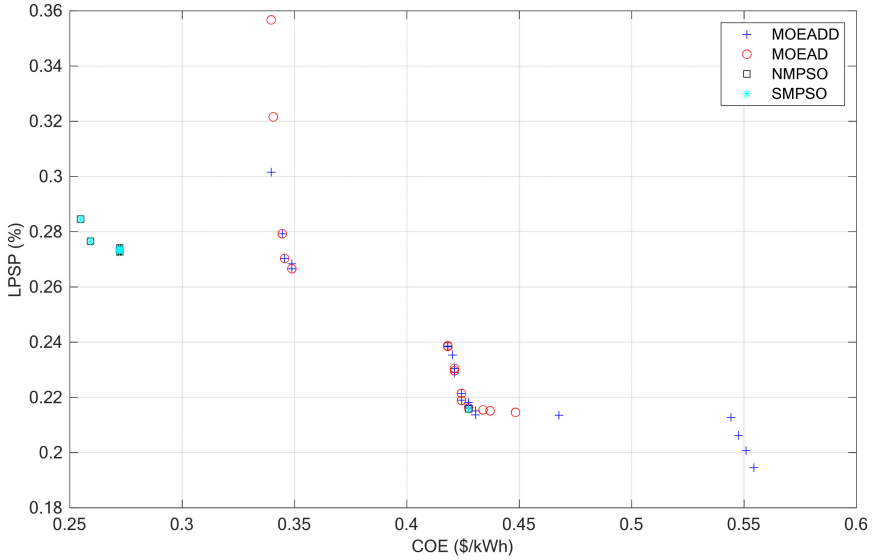

Figure 10. Comparison of PFs obtained for CASE 1 using different algorithms.

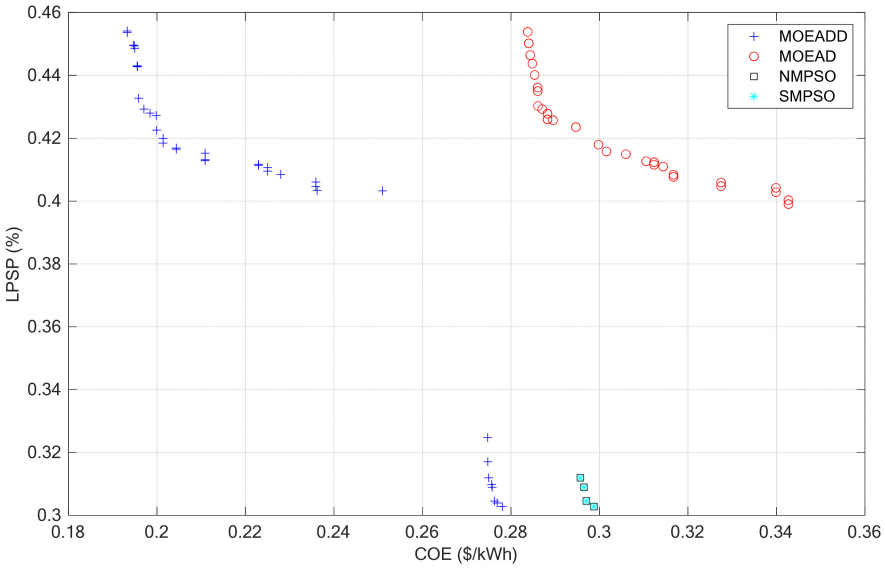

Figure 11. Comparison of PFs obtained for CASE 2 using different algorithms.

For CASE 1, MOEA/DD, MOEA/D, NMPSO and SMPSO generated a set of 23 solutions, 15 solutions, 11 solutions and 11 solutions, respectively. When these results were compared to each other to determine which solutions were nondominated, it was found that:

- Among the 23 solutions generated using MOEA/DD, 16 were nondominated by any other solutions found using the remaining algorithms.

- Among the 15 solutions generated using MOEA/D, 5 were nondominated by any other solutions found using the remaining algorithms.
- Among the 11 solutions generated using NMPSO, all were dominated by the solutions found using the remaining algorithms.
- All 11 solutions generated using SMPSO were nondominated.

For CASE 2, the four used algorithms—MOEA/DD, MOEA/D, NMPSO and SMPSO—generated 37 solutions, 28 solutions, 4 solutions, and 4 solutions, respectively. These results were compared to each other to determine which solutions were nondominated. In this case, (i.e., they are part of the PF), the 37 solutions generated using MOEA/DD were nondominated by any other solutions found using the remaining algorithms. In contrast, all solutions generated using MOEA/D, NMPSO and SMPSO were dominated by those obtained using the MOEA/DD.

Therefore, it can be concluded that the proposed approach, using MOEA/DD, is the most performant one for both operation modes. This conclusion was verified in the microgrid operation mode case (i.e., CASE 2.).

7. Conclusions

This paper presents a dominance and decomposition-based multi-objective evolutionary algorithm to optimize a hybrid nanogrid/microgrid's size and operation. Hafr Al-Batin, a city of the Eastern Province of Saudi Arabia, was selected for implementation. The reason behind choosing that particular city is the common practice of using desert camps, which can easily be considered nanogrid units. The nanogrid consisted of a solar system, storage batteries, diesel generators, invertor, and load components. Two different modes of operation were investigated in this paper: one with the single nanogrid and the second a combination of nanogrids, coordinated to form a microgrid. In the formulation of the optimization problem, the reliability and the cost of the system were considered. A set of diverse, acceptable, and widespread solutions were obtained from the developed program for both the case studies, which will guide the designer/operator of a nanogrid/microgrid to model such a system. The obtained results offered competitive and practical solutions to the addressed problem using a multi-objective optimization strategy.

However, the addressed issue of desert camping is not a regional problem; rather, it can be implemented in any part of the world. The designed nanogrid/microgrid concept applies to desert camps, but is suitable for any islanded load of a similar kind. Moreover, using such desert camps is widely seen in all the world's desert areas, particularly in the Gulf countries. Therefore, the paper's aspect is global, even though it addresses a particular region of the globe.

The presented work can be further continued to investigate possible recovery strategies, subject to the failure of a source like a PV panel or diesel generator. The effect of ageing on associated equipment (PV system, diesel generator, batteries, inverter, etc.) or of equipment modification (due to the connection of a new tent, for example) of load size can be considered future work of this research.

Author Contributions: Conceptualization, H.R.A.-H.B. and M.S.S.; methodology, H.R.A.-H.B. and M.S.J.; software, H.R.A.-H.B.; validation, H.R.A.-H.B. and M.A.M.R.; formal analysis, M.S.S., M.S.J. and Y.A.S.; investigation, H.R.A.-H.B., M.S.J., M.S.S., and Y.A.S.; resources, M.S.S., H.R.A.-H.B., M.S.J. and Y.A.S.; data curation, H.R.A.-H.B.; writing—original draft preparation, H.R.A.-H.B., M.S.S., M.S.J. and Y.A.S.; writing—review and editing, H.R.A.-H.B., M.S.S., M.S.J., Y.A.S. and M.A.M.R.; visualization, H.R.A.-H.B., M.S.S., M.S.J. and M.A.M.R.; supervision, H.R.A.-H.B. and M.A.M.R.; project administration, H.R.A.-H.B.; funding acquisition, H.R.A.-H.B. All authors have read and agreed to the published version of the manuscript.

Funding: This research was funded by DEANSHIP OF SCIENTIFIC RESEARCH, UNIVERSITY OF HAFR AL BATIN, grant number G-109-2020.

Acknowledgments: The authors extend their appreciation to the Deanship of Scientific Research, University of Hafr Al-Batin, for funding this work through the research group project No G-109-2020.

Conflicts of Interest: The authors declare no conflict of interest.

Appendix A

Table A1. PV panels models and information [54].

Model #	Name	YPV	Efficiency	α_P	Tc_{NOCT}	Cost	US$/Watt
Model # 1	Kyocera Solar (KC200)	200.00	0.20	−0.46	47.00	800.00	$4.00
Model # 2	BP Solar (SX 170B)	170.00	0.17	−0.46	47.00	728.97	$4.29
Model # 3	Evergreen (Spruce ES-170)	170.00	0.17	−0.46	47.00	731.00	$4.30
Model # 4	Evergreen (Spruce ES-180)	180.00	0.18	−0.46	47.00	774.00	$4.30
Model # 5	Evergreen (Spruce ES-190)	190.00	0.19	−0.46	47.00	817.00	$4.30
Model # 6	Solar World (SW-165)	165.00	0.17	−0.46	47.00	709.97	$4.30
Model # 7	Mitsubishi (PV-MF155EB3)	155.00	0.16	−0.46	47.00	669.97	$4.32
Model # 8	Sharp (ND-208U1)	208.00	0.21	−0.46	47.00	898.56	$4.32
Model # 9	Sharp (NE-170U1)	170.00	0.17	−0.46	47.00	739.50	$4.35
Model # 10	Mitsubishi (PV-MF165EB4)	165.00	0.17	−0.46	47.00	719.97	$4.36
Model # 11	Sunwize (SW150)	150.00	0.15	−0.46	47.00	668.31	$4.46
Model # 12	Kyocera (KC175GT)	175.00	0.18	−0.46	47.00	799.00	$4.57
Model # 13	Kyocera (KC175GT)	175.00	0.18	−0.46	47.00	799.00	$4.57

Table A2. Batteries models and information [54].

Model #	Name	Efficiency	Capacity	Voltage	Cost	Lifetime	Weight (lbs)
Model # 1	MK 8L16	0.85	370.00	6.00	288.77	12.00	113.00
Model # 2	Surrette 12-Cs-11Ps	0.85	357.00	12.00	1118.96	12.00	272.00
Model # 3	Surrette 2Ks33Ps	0.85	1765.00	2.00	874.90	12.00	208.00
Model # 4	Surrette 4-CS-17PS	0.85	546.00	4.00	604.23	12.00	128.00
Model # 5	Surrette 4-Ks-21Ps	0.85	1104.00	4.00	1110.44	12.00	267.00
Model # 6	Surrette 4-Ks-25Ps	0.85	1350.00	4.00	1386.85	12.00	315.00
Model # 7	Surrette 6-Cs-17Ps	0.85	546.00	6.00	906.31	12.00	221.00
Model # 8	Surrette 6-Cs-21Ps	0.85	683.00	6.00	1075.01	12.00	271.00
Model # 9	Surrette 6-Cs-25Ps	0.85	820.00	6.00	1241.37	12.00	318.00
Model # 10	Surrette 8-Cs-17Ps	0.85	546.00	8.00	1256.21	12.00	294.00

Table A2. *Cont.*

Model #	Name	Efficiency	Capacity	Voltage	Cost	Lifetime	Weight (lbs)
Model # 11	Surrette 8-Cs-25Ps	0.85	820.00	8.00	1654.76	12.00	424.00
Model # 12	Surrette S-460	0.85	350.00	6.00	324.93	12.00	117.00
Model # 13	Surrette S-530	0.85	400.00	6.00	370.65	12.00	127.00
Model # 14	Trojan L16H	0.85	420.00	6.00	357.00	12.00	121.00
Model # 15	Trojan T-105	0.85	225.00	6.00	138.00	12.00	62.00
Model # 16	US Battery US185	0.85	195.00	12.00	216.58	12.00	111.00
Model # 17	US Battery Us2200	0.85	225.00	6.00	127.99	12.00	63.00
Model # 18	US Battery US250	0.85	250.00	6.00	126.35	12.00	72.00
Model # 19	Surrette S-460	0.85	350.00	6.00	357.36	12.00	117.00
Model # 20	Surrette S-530 6V	0.85	400.00	6.00	406.09	12.00	127.00
Model # 21	Surrette 4-CS-17PS	0.85	546.00	4.00	770.45	12.00	128.00
Model # 22	Surrette 4-Ks-21Ps	0.85	1104.00	4.00	1206.00	12.00	267.00
Model # 23	Surrette 4-Ks-25Ps	0.85	1350.00	4.00	1508.83	12.00	315.00
Model # 24	Surrette 6-Cs-17Ps	0.85	546.00	6.00	932.31	12.00	221.00
Model # 25	Surrette 6-Cs-21Ps	0.85	683.00	6.00	1164.00	12.00	271.00
Model # 26	Surrette 6-Cs-25Ps	0.85	820.00	6.00	1349.45	12.00	318.00
Model # 27	Surrette 8-Cs-17Ps	0.85	820.00	8.00	1795.71	12.00	424.00

Table A3. Inverters models and information [54].

Model #	Inverter Manufacture	Model	Price ($)	Power (W)	Input Voltage (VDC)	Output Voltage (VAC)	Nominal Frequency (Hz)	Efficiency
Model # 1	Xantrex (XW6048)	XW6048	3597.75	6000	48	120	60	0.92
Model # 2	Xantrex (XW4548)	XW4548	2878.2	4500	48	120	60	0.92
Model # 3	Xantrex (SW5548)	SW5548	2735.85	5500	48	120	60	0.92
Model # 4	Xantrex (SW4048)	SW4048	2178.96	4000	48	120	60	0.92
Model # 5	Outback (GTFX3048)	GTFX3048	1760	3000	48	120	60	0.92

Table A3. *Cont.*

Model #	Inverter Manufacture	Model	Price ($)	Power (W)	Input Voltage (VDC)	Output Voltage (VAC)	Nominal Frequency (Hz)	Efficiency
Model # 6	Outback (GVFX3648)	GVFX3648	1913	3600	48	120	60	0.92
Model # 7	Sunny Island (SI4248U)	SI4248U	4228	4200	48	120	60	0.92
Model # 8	Sunny Island (SI5048U)	SI5048U	6535	5000	48	120	60	0.92

References

1. Shaqour, A.; Farzaneh, H.; Yoshida, Y.; Hinokuma, T. Power control and simulation of a building integrated stand-alone hybrid PV-wind-battery system in Kasuga City, Japan. *Energy Rep.* **2020**, *6*, 1528–1544. [CrossRef]
2. Basak, P.; Chowdhury, S.; Dey, S.H.N.; Chowdhury, S.P. A literature review on integration of distributed energy resources in the perspective of control, protection and stability of microgrid. *Renew. Sustain. Energy Rev.* **2012**, *16*, 5545–5556. [CrossRef]
3. Krishan, O.; Suhag, S. An updated review of energy storage systems: Classification and applications in distributed generation power systems incorporating renewable energy resources. *Int. J. Energy Res.* **2019**, *43*, 6171–6210. [CrossRef]
4. Farmanbar, M.; Parham, K.; Arild, Ø.; Rong, C. A Widespread Review of Smart Grids Towards Smart Cities. *Energies* **2019**, *12*, 4484. [CrossRef]
5. Unamuno, E.; Barrena, J.A. Hybrid ac/dc microgrids—Part I: Review and classification of topologies. *Renew. Sustain. Energy Rev.* **2015**, *52*, 1251–1259. [CrossRef]
6. Burmester, D.; Rayudu, R.; Seah, W.; Akinyele, D. A review of nanogrid topologies and technologies. *Renew. Sustain. Energy Rev.* **2017**, *67*, 760–775. [CrossRef]
7. Mostafa, M.H.; Aleem, S.H.E.A.; Ali, S.G.; Ali, Z.M.; Abdelaziz, A.Y. Techno-economic assessment of energy storage systems using annualized life cycle cost of storage (LCCOS) and levelized cost of energy (LCOE) metrics. *J. Energy Storage* **2020**, *29*, 101345. [CrossRef]
8. Burmester, D. Nanogrid topology, control and interactions in a microgrid structure. Ph.D. Thesis, Victoria University of Wellington, Wellington, New Zealand, 2018.
9. Adda, R.; Ray, O.; Mishra, S.; Joshi, A. DSP based PWM control of Switched Boost Inverter for DC nanogrid applications. In Proceedings of the IECON 2012-38th Annual Conference on IEEE Industrial Electronics Society, Montreal, QC, Canada, 25–28 October 2012; pp. 5285–5290.
10. Nag, S.S.; Adda, R.; Ray, O.; Mishra, S.K. Current-Fed Switched Inverter based hybrid topology for DC Nanogrid application. In Proceedings of the IECON 2012-38th Annual Conference on IEEE Industrial Electronics Society, Vienna, Austria, 10–13 November 2013; pp. 7146–7151.
11. Atia, R.; Yamada, N. Sizing and Analysis of Renewable Energy and Battery Systems in Residential Microgrids. *IEEE Trans. Smart Grid* **2016**, *7*, 1204–1213. [CrossRef]
12. Majidi, M.; Nojavan, S.; Esfetanaj, N.N.; Najafi-Ghalelou, A.; Zare, K. A multi-objective model for optimal operation of a battery/PV/fuel cell/grid hybrid energy system using weighted sum technique and fuzzy satisfying approach considering responsible load management. *Sol. Energy* **2017**, *144*, 79–89. [CrossRef]
13. Lan, H.; Wen, S.; Hong, Y.Y.; Yu, D.C.; Zhang, L. Optimal sizing of hybrid PV/diesel/battery in ship power system. *Appl. Energy* **2015**, *158*, 26–34. [CrossRef]
14. Lokeshgupta, B.; Sivasubramani, S. Multi-objective home energy management with battery energy storage systems. *Sustain. Cities Soc.* **2019**, *47*, 101458. [CrossRef]
15. Li, L.; Liu, P.; Li, Z.; Wang, X. A multi-objective optimization approach for selection of energy storage systems. *Comput. Chem. Eng.* **2018**, *115*, 213–225. [CrossRef]
16. Hosseinalizadeh, R.; Shakouri, H.; Amalnick, M.S.; Taghipour, P. Economic sizing of a hybrid (PV-WT-FC) renewable energy system (HRES) for stand-alone usages by an optimization-simulation model: Case study of Iran. *Renew. Sustain. Energy Rev.* **2016**, *54*, 139–150. [CrossRef]
17. Brandoni, C.; Renzi, M. Optimal sizing of hybrid solar micro-CHP systems for the household sector. *Appl. Therm. Eng.* **2015**, *75*, 896–907. [CrossRef]
18. Wang, R.; Xiong, J.; He, M.; Gao, L.; Wang, L. Multi-objective optimal design of hybrid renewable energy system under multiple scenarios. *Renew. Energy* **2020**, *151*, 226–237. [CrossRef]
19. Shivam, K.; Tzou, J.-C.; Wu, S.-C. Multi-Objective Sizing Optimization of a Grid-Connected Solar–Wind Hybrid System Using Climate Classification: A Case Study of Four Locations in Southern Taiwan. *Energies* **2020**, *13*, 2505. [CrossRef]
20. Dahiru, A.T.; Tan, C.W. Optimal sizing and techno-economic analysis of grid-connected nanogrid for tropical climates of the Savannah. *Sustain. Cities Soc.* **2020**, *52*, 101824. [CrossRef]

21. Mazzeo, D.; Matera, N.; de Luca, P.; Baglivo, C.; Congedo, P.M.; Oliveti, G. Worldwide geographical mapping and optimization of stand-alone and grid-connected hybrid renewable system techno-economic performance across Köppen-Geiger climates. *Appl. Energy* **2020**, *276*, 115507. [CrossRef]
22. Nömm, J.; Rönnberg, S.; Bollen, M. An Analysis of Voltage Quality in a Nanogrid during Islanded Operation. *Energies* **2019**, *12*, 614. [CrossRef]
23. Tellbach, D.; Li, Y.-F. Cyber-Attacks on Smart Meters in Household Nanogrid: Modeling, Simulation and Analysis. *Energies* **2018**, *11*, 316. [CrossRef]
24. Al-falahi, M.D.A.; Jayasinghe, S.D.G.; Enshaei, H. A review on recent size optimization methodologies for standalone solar and wind hybrid renewable energy system. *Energy Convers. Manag.* **2017**, *143*, 252–274. [CrossRef]
25. Hilden, J.T. *Bedouin Weaving of Saudi Arabia and its Neighbours*; Arabian Publishing: Surbiton, UK, 2010.
26. Li, K.; Deb, K.; Zhang, Q.; Kwong, S. An evolutionary many-objective optimization algorithm based on dominance and decomposition. *IEEE Trans. Evol. Comput.* **2015**, *19*, 694–716. [CrossRef]
27. Belgana, A.; Rimal, B.P.; Maier, M. Open Energy Market Strategies in Microgrids: A Stackelberg Game Approach Based on a Hybrid Multiobjective Evolutionary Algorithm. *IEEE Trans. Smart Grid* **2015**, *6*, 1243–1252. [CrossRef]
28. Latreche, Y.; Bouchekara, H.R.E.H.; Javaid, M.S.; Shahriar, M.S.; Sha'aban, Y.A.; Kerrour, F. Optimal siting and sizing of DG units using a decomposition based multiobjective evolutionary algorithm. In Proceedings of the International Conference in Artificial Intelligence in Renewable Energetic Systems, Tipasa, Algeria, 22–24 December 2020; Volume 174, pp. 521–532.
29. Bouchekara, H.R.E.H.; Javaid, M.S.; Shaaban, Y.A.; Shahriar, M.S.; Ramli, M.A.M.; Latreche, Y. Decomposition based multiobjective evolutionary algorithm for PV/Wind/Diesel Hybrid Microgrid System design considering load uncertainty. *Energy Rep.* **2021**, *7*, 52–69. [CrossRef]
30. Vazquez, A.; Martin, K.; Arias, M.; Sebastian, J. On Bidirectional DC Nano-Grids: Design Considerations and an Architecture Proposal. *Energies* **2019**, *12*, 3715. [CrossRef]
31. Rezk, H.; Fathy, A.; Aly, M. A robust photovoltaic array reconfiguration strategy based on coyote optimization algorithm for enhancing the extracted power under partial shadow condition. *Energy Rep.* **2021**, *7*, 109–124. [CrossRef]
32. Yamada, M. *Vision 2030 and the Birth of Saudi Solar Energy*; Middle East Institute: Washington, DC, USA, 2016.
33. Daud, A.K.; Ismail, M.S. Design of isolated hybrid systems minimizing costs and pollutant emissions. *Renew. Energy* **2012**, *44*, 215–224. [CrossRef]
34. Razmjoo, A.; Shirmohammadi, R.; Davarpanah, A.; Pourfayaz, F.; Aslani, A. Stand-alone hybrid energy systems for remote area power generation. *Energy Rep.* **2019**, *5*, 231–241. [CrossRef]
35. El-Hefnawi, S.H. Photovoltaic diesel-generator hybrid power system sizing. *Renew. Energy* **1998**, *13*, 33–40. [CrossRef]
36. Ashari, M.; Nayar, C.V. An optimum dispatch strategy using set points for a photovoltaic (PV)-diesel-battery hybrid power system. *Sol. Energy* **1999**, *66*, 1–9. [CrossRef]
37. Azoumah, Y.; Yamegueu, D.; Ginies, P.; Coulibaly, Y.; Girard, P. Sustainable electricity generation for rural and peri-urban populations of sub-Saharan Africa: The 'flexy-energy' concept. *Energy Policy* **2011**, *39*, 131–141. [CrossRef]
38. Souraki, H.P.; Radmehr, M.; Rezanejad, M. Distributed energy storage system-based control strategy for hybrid DC/AC microgrids in grid-connected mode. *Int. J. Energy Res.* **2019**, *43*, 6283–6295. [CrossRef]
39. Parida, A.; Chatterjee, D. Stand-alone AC-DC microgrid-based wind-solar hybrid generation scheme with autonomous energy exchange topologies suitable for remote rural area power supply. *Int. Trans. Electr. Energy Syst.* **2018**, *28*, e2520. [CrossRef]
40. Sarangi, S.; Sahu, B.K.; Rout, P.K. Distributed generation hybrid AC/DC microgrid protection: A critical review on issues, strategies, and future directions. *Int. J. Energy Res.* **2020**, *44*, 3347–3364. [CrossRef]
41. Kaabeche, A.; Belhamel, M.; Ibtiouen, R. Techno-economic valuation and optimization of integrated photovoltaic/wind energy conversion system. *Sol. Energy* **2011**, *85*, 2407–2420. [CrossRef]
42. Yang, H.; Zhou, W.; Lu, L.; Fang, Z. Optimal sizing method for stand-alone hybrid solar-wind system with LPSP technology by using genetic algorithm. *Sol. Energy* **2008**, *82*, 354–367. [CrossRef]
43. Wang, R. Multi-objective configuration optimization method for a diesel-based hybrid energy system. *Energy Rep.* **2020**, *6*, 2146–2152. [CrossRef]
44. Alnaser, W.E.; Alnaser, N.W. The Impact of the Rise of Using Solar Energy in GCC Countries. *Renew. Energy Environ. Sustain.* **2020**, *4*, 167–183.
45. Alharbi, F.; Csala, D. Saudi Arabia's Solar and Wind Energy Penetration: Future Performance and Requirements. *Energies* **2020**, *13*, 588. [CrossRef]
46. Solar Resource Maps and GIS Data for 200+ Countries | Solargis. Available online: https://solargis.com/maps-and-gis-data/download/saudi-arabia (accessed on 29 August 2020).
47. JRC Photovoltaic Geographical Information System (PVGIS)-European Commission. Available online: https://re.jrc.ec.europa.eu/pvg_tools/en/tools.html (accessed on 11 February 2021).
48. Deb, K.; Jain, H. An evolutionary many-objective optimization algorithm using reference-point-based nondominated sorting approach, Part I: Solving problems with box constraints. *IEEE Trans. Evol. Comput.* **2014**, *18*, 577–601. [CrossRef]
49. Das, I.; Dennis, J.E. Normal-boundary intersection: A new method for generating the Pareto surface in nonlinear multicriteria optimization problems. *SIAM J. Optim.* **1998**, *8*, 631–657. [CrossRef]

50. Deb, K.; Pratap, A.; Agarwal, S.; Meyarivan, T. A Fast and Elitist Multiobjective Genetic Algorithm: NSGA-II. *IEEE Trans. Evol. Comput.* **2002**, *6*, 182–197. [CrossRef]
51. Deb, K.; Agrawal, R.B.; Agrawal, R.B. Simulated binary crossover for continuous search space. *Complex Syst.* **1995**, *9*, 115–148.
52. Deb, K.; Deb, K.; Goyal, M. A Combined Genetic Adaptive Search (GeneAS) for Engineering Design. *Comput. Sci. Inf.* **1996**, *26*, 30–45.
53. Li, K.; Deb, K.; Zhang, Q.; Zhang, Q. Efficient Nondomination Level Update Method for Steady-State Evolutionary Multiobjective Optimization. *IEEE Trans. Cybern.* **2017**, *47*, 2838–2849. [CrossRef] [PubMed]
54. Rios-Rivera, M. Small Wind/Photovoltaic Hybrid Renewable Energy System Optimization. Master's Thesis, University of Puerto Rico, San Juan, Puerto Rico, 2008.